frontiers in Physics

ORIGINAL RESEARCH
published: 04 October 2021
doi: 10.3389/fphy.2021.740627

Confined Monolayer Ice Between CaF_2 (111) and Graphene: Structure and Stability

*Shi-Qi Li, Shi Qiu, Hongsheng Liu, Maodu Chen and Junfeng Gao**

Key Laboratory of Materials Modification by Laser, Ion and Electron Beams, Dalian University of Technology, Ministry of Education, Dalian, China

Water monolayer can form in layered confined systems. Here, CaF_2 (111) and graphene are chosen as modeling systems to explore the structure and stability of confined monolayer water. First, water molecules tend to intercalate into a confined space between graphene and CaF_2, rather than on a bare surface of graphene. Water molecules can move fast in the confined space due to a low diffusion barrier. These water molecules are likely to aggregate together, forming monolayer ice. Four ice phases including ice II, ice III, ice IV, and ice Ih are compared in this confined system. Intriguingly, all the ice phases undergo very small deformation, indicating the 2D monolayer ice can be stable in the CaF_2–graphene–confined system. Beyond, projected band structures are also plotted to understand the electronic behavior of these confined ice phases. Nearly all the bands originated from confined ices are flat and locate about 2–3 eV below the Fermi level. Binding energy calculations suggest that the stability sequence in this confined system as follows: Ih-up ≈ Ih-down ≈ II < IV < III. Our results bring new insights into the formation of water monolayer production in such a confined condition.

Keywords: structure and stability, confined water, graphene, ice phases, first-principle calculations

OPEN ACCESS

Edited by:
Wenxiang Xu,
Hohai University, China

Reviewed by:
Haifei Zhan,
Zhejiang University, China
Dengfeng Li,
Chongqing University of Posts and Telecommunications, China

****Correspondence:***
Junfeng Gao
gaojf@dlut.edu.cn

Specialty section:
This article was submitted to Condensed Matter Physics, a section of the journal Frontiers in Physics

Received: *13 July 2021*
Accepted: *30 August 2021*
Published: *04 October 2021*

Citation:
Li S-Q, Qiu S, Liu H, Chen M and Gao J (2021) Confined Monolayer Ice Between CaF_2 (111) and Graphene: Structure and Stability. Front. Phys. 9:740627. doi: 10.3389/fphy.2021.740627

INTRODUCTION

The behavior of water at surfaces and a nanoconfined space [1] in two, three, or one dimensions is significantly different from that in bulk ice [2–4]. Understanding the structural tendencies of nanoconfined water is of great interest in biology [5], material science [6–8], nanofluidics [9], tribology, and, most recently, electronics [10, 11]. Because of various possible hydrogen bond networks, the structure of water is notoriously perplexed [12], rising as one of the most challenging issues in the 21st century [13]. The subtle interplay between the water–substrate and water–water interactions brings about many new distinctive ice configurations on different substrates [14–18]. In vacuum and on weakly interacting substrates, Xu et al. [14] found a helical ice monolayer with every six water molecules helically arranged along the normal of the basal plane by performing an intensive structural search based on ab initio calculations. On Au(111), a two-dimensional (2D) interlocked ice consisting of two flat hexagonal water layers in which the hexagons in two sheets are in registry is imaged by non-contact atomic force microscopy and identified by density functional calculations [15].

Except for various types of monolayer ice formed on surfaces, 2D monolayer-confined ice also has drawn much attention due to its relevance to a series of processes in nature and industry [19]. Nevertheless, the structures of 2D monolayer ice under distinct confinements are still under debate.

Recently, by performing scanning probe microscopy (SPM), graphene ultrathin coatings are utilized to assist the visualization of interfacial water adlayers. This made remarkable progress on interfacial water. Xu et al. [20] observed water adlayers on mica coated by monolayer graphene at room temperature by using atomic force microscopy. The graphene coating can stably "fix" the water adlayer structures, thus permitting the detection of the structure of the first water adlayers under ambient conditions [21]. Therefore, the presence of ambient water adlayers between graphene [19] and various substrates, including mica [11, 21–24], SiO_2 [25, 26], BaF_2 [27], SiC [28], sapphire [29], Ni [30], Ru, Cu [31], and Si [32], has been widely studied by experimental probing techniques. Taking mica as an example, the structure of the first wetting adlayer confined between graphene and mica is unique, quite different from ice Ih, due to strong mica–water interaction [21]. The structural characteristics of intercalated water adlayers between graphene and mica under a thermal treatment were also investigated by Ochedowski et al [22]. They showed that the intercalated water adlayers are partially removed under mild heating (200°C), and the defect density increases, leading to "nanoblister" formation at a temperature of 600°C, causing a transition from the p-type to n-type for graphene layers [22].

CaF_2 (111)/graphene is an excellent platform to trap water molecules and generate confined ice layers. Recently, the formation of a several monolayer thick hydration layer on a graphene-coated hydrophilic substrate CaF_2 (111) was revealed [33]. The first layer is so stable that it cannot be removed upon heating. After this, hydration layers confined between graphene and the CaF_2 substrate were found to electronically modify graphene as the material's electron density transfers from graphene to the hydration layer [34]. However, the structure and stability of monolayer ice confined between CaF_2 (111) and graphene remain unclear. In an experiment, many factors can influence the hydration layers and properties of graphene [35], such as the types of adhesive tapes [23], other adsorbents [22], and additives. So a theoretical study on structural information and stability of water confined between graphene and CaF_2 at the atomic level is urgently needed.

In this study, the structure and stability of monolayer ice confined between CaF_2 (111) and graphene are investigated systematically based on first-principles calculations. Water molecules tend to aggregate together to form monolayer ice. A water molecule will automatically move to the "edge" of the top surface of the ice layer, promoting monolayer ice growth and prohibiting multilayer nucleation. Beyond, the energy barrier for water diffusion between CaF_2 (111) and graphene is very low. Thus, water molecule can move freely and connect with each other into a monolayer ice between CaF_2 (111) and graphene. Four probable ice phase structures including ice II, ice III, ice IV, and ice Ih are studied in our confined system. All the ice phases are maintained with only small deformations in the CaF_2–graphene–confined system. Binding energy suggests that the most stable monolayer ice confined between CaF_2 (111) and graphene is phase-III. Confined ice III is thermodynamically stable under a wide temperature and pressure span according to the calculated phase diagram. Furthermore, the band structures of these systems are plotted to explore the electronic properties of confined ice phases. The bands originated from confined ice are flat and locate about 2–3 eV below the Fermi level.

METHODS

All the first-principles calculations are based on the DFT, which is implanted in the Vienna ab initio simulation package code (VASP) [36]. The Perdew–Burke–Ernzerhof version of the generalized gradient approximation (GGA-PBE) was chosen as the exchange-correlation functional [37] along with the dispersion correction introduced by Grimme (PBE + D3) [38]. In this work, all atoms were fully relaxed using DFT with vdW correction to obtain the equilibrium distance. The electron wave functions are solved with plane wave basis set in conjunction with pseudo potentials by the projector augmented wave (PAW) method [39]. The K points in the first Brillouin zone (BZ) are generated in the form of a Monkhorst–Pack $4 \times 4 \times 1$ grid [40]. A 500 eV kinetic cutoff energy was used for the plane wave basis. The structure of water confined between CaF_2 (111) and graphene were optimized using standard local optimization algorithms with convergence criteria of 10^{-4} eV for both electronic and ionic relaxation. In our CaF_2 surface slab, there is a net dipole along the Z direction, which will introduce an artificial electric field in calculations with periodic boundary conditions (PBC), and the dipole correction scheme introduced by Neugebauer and Scheffler is applied in all calculations [41, 42]. To avoid spurious interactions between neighboring structures in the tetragonal supercell, a vacuum layer of 25 Å was included in all non-periodic directions.

The surface lattice of CaF_2 (111) is 3.86 Å, which is in good agreement with prior studies, and the CaF_2 (111) surface slab is terminated with fluorine atoms and composed by two F-Ca-F triple layers. The lattice of graphene is 2.46 Å. All the ice structures including ice II, ice III, and ice IV are from MD simulations [43], which will be intercalated between CaF_2 (111) and graphene. We choose 4×4 CaF_2 (111)/3×3 ice II/6×6 graphene, 3×3 CaF_2 (111)/2×2 ice III/5×5 graphene, 4×4 CaF_2 (111)/$1 \times \sqrt{3}$ ice IV/6×6 graphene, and 4×4 CaF_2 (111)/3×3 ice Ih/6×6 graphene to construct the confined systems. The lattice mismatch of these supercells is 4.4, 5.9, 8.1, and 8.1% for CaF_2 (111)/ice II/graphene, CaF_2 (111)/ice III/graphene, CaF_2 (111)/ice IV/graphene, and CaF_2 (111)/ice Ih/graphene, respectively.

Water molecule diffusion barriers are calculated *via* the climbing image–nudged elastic band (CI-NEB) [44] method. This technique can efficiently map the minimum energy path and find the saddle points between two given local minima for the system. Six intermediate images are used in CI-NEB calculations. Each image was relaxed until the forces on the atom were less than 0.02 eV/Å.

The binding energies of monolayer ice phases between the CaF_2 and the graphene system are calculated as follows:

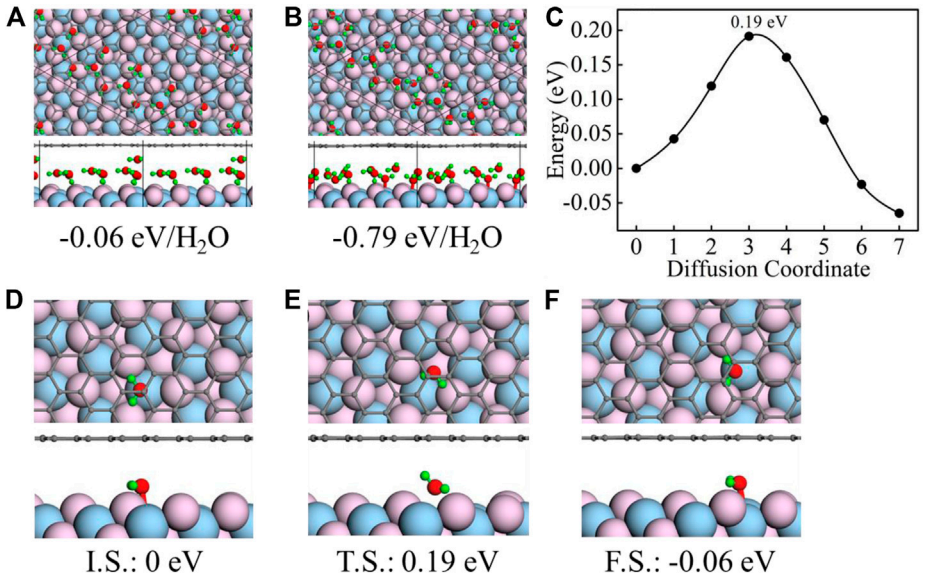

FIGURE 1 | Initial **(A)** and final **(B)** geometric structures for the stratification test along with their corresponding binding energies. **(C)** Calculated energy barriers for water molecule diffusion between CaF_2 (111) and graphene. **(D–F)** Top- and side-view geometric structures of the initial state (I.S.) **(D)**, transition state (T.S.) **(E)**, and final state (F.S.) **(F)** of water molecule diffusion between CaF_2 (111) and graphene. The total energies for I.S., T.S., and F.S. are all denoted in the bottom as a reference of I.S. In all panels, the black, red, green, flesh pink, and light blue spheres represent the C, O, H, F, and Ca atoms, respectively.

$$E_b = [\mathrm{E(Total)} - \mathrm{E}(CaF_2) - \mathrm{E(Graphene)} - \mathrm{N}(H_2O) * \mathrm{E}(H_2O)]/\mathrm{N}(H_2O), \quad (1)$$

where E(Total), E(CaF_2), E(Graphene), and E(H_2O) is total energy of the CaF_2/H_2O/graphene system, a clean CaF_2(111), graphene sheet, and an isolated water molecule, respectively.

RESULTS AND DISCUSSION

Stratification Test and NEB Calculations

CaF_2 (111)–graphene is an excellent platform to trap water [33, 34]. These water molecules are likely to aggregate together forming monolayer connecting with each other by hydrogen bonding. We perform stratification test to make certain the confined ice is monolayer or not. As shown in **Figure 1A**, we put a water molecule on top of the monolayer water structure confined between CaF_2 (111) and graphene. After optimization, the water molecule move to the edge of the existing water structure forming a new monolayer (**Figure 1B**). This process is barrierless, during which the binding energy decrease by 0.73 eV/H_2O. Therefore, the confined ice between CaF_2 (111) and graphene must be monolayer.

Furthermore, the water molecule diffusion between CaF_2 (111) and graphene is investigated using the CI-NEB method. As shown in **Figure 1C**, the water diffusion energy barrier is 0.19 eV from initial adsorption local minima (I.S., **Figure 1D**) to final adsorption local minima (F.S., **Figure 1F**). During this process, the water molecule is first locates on the top of Ca atom (**Figure 1D**), then moves to the hollow site (**Figure 1E**), and finally locates on the top of the neighboring Ca atom (**Figure 1F**). Choosing the total energy of the I.S. system as a reference, the energy of F.S. and T.S. are all listed in the **Figures 1E,F** (0.19 eV and −0.06 eV). The speed of water diffusion can be characterized by the water diffusion coefficient D_{H_2O} which can be estimated from the diffusion barriers by the following formula:

$$D_{H_2O} = a^2 \nu exp\left(\frac{-\Delta E}{K_B T}\right), \quad (2)$$

where a is the distance of the hop along the diffusion pathway and ν is the attempt frequency, about 10^{13} Hz, which is generally in the range of phonon frequencies [45, 46]. ΔE is the diffusion energy barrier [45]. K_B is the Boltzmann constant and T represents the temperature. According to the diffusion results, at room temperature (T = 300 K), the water diffusion coefficient D_{H_2O} is calculated as 8.35×10^{-6} cm^2/s. The low diffusion energy barrier and high diffusion speed of water molecule provide strong evidence for monolayer ice formation between CaF_2 (111) and graphene.

Structure and Stability of Confined Ice

Four monolayer ice phases including Ice II [43], III [43], IV [43], and Ih are intercalated between CaF_2 (111) and graphene. All the free-standing structures of the four ice phases are depicted in the **Supplementary Figure S1** in Supporting Information. For ice I_h, two cases in which H atoms pointing to CaF_2 (Ih-down) or graphene (Ih-up) are all considered. The optimized results are shown in the **Figures 2A–E**.

The monolayer ice II has a planar hexagonal morphology, and it is made up of two kinds of water molecules with different orientations. The plane of every water molecule is perpendicular to the planes of three nearest-neighbor molecules. Besides, the

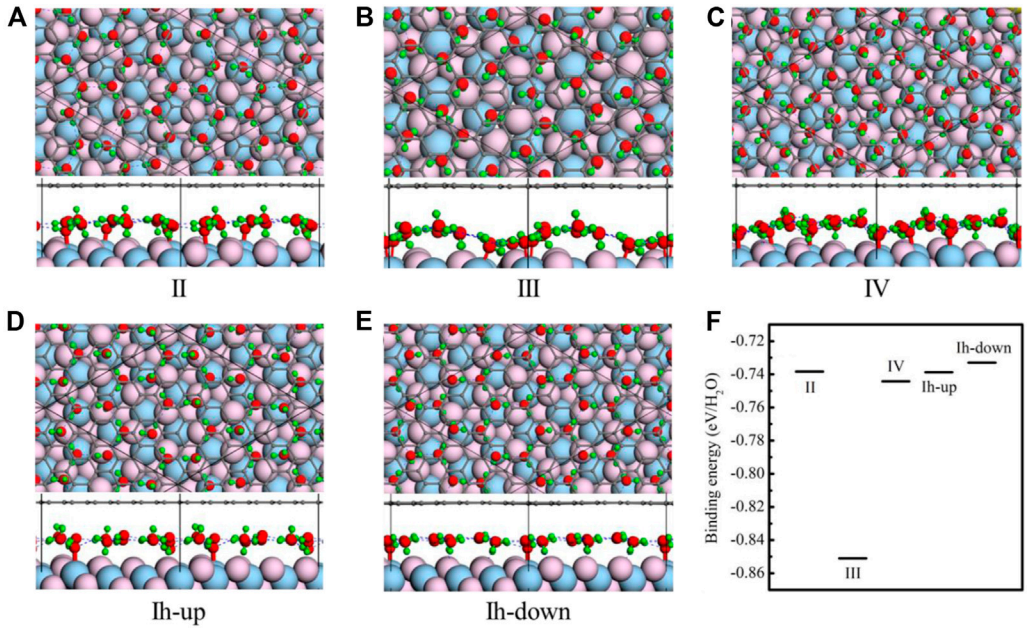

FIGURE 2 | Structures of five ice phases including ice II **(A)**, III **(B)**, IV **(C)**, and Ih **(D,E)** confined between CaF_2(111) and graphene. According to the different orientations of OH, ice Ih can be classified into two kinds. In all panels, the black, red, green, flesh pink, and light blue spheres represent the C, O, H, F, and Ca atoms, respectively. **(F)** The binding energies of monolayer ice phases between the CaF_2 and the graphene system. Light blue spheres represent the C, O, H, F, and Ca atoms, respectively.

monolayer ice II displays considerable net polarization because all the dipole vectors of water molecules are parallel to the longest diagonal of a hexagon. As shown in **Figure 2A**, under confinement of graphene and CaF_2 (111), the structural motifs of ice II change slightly. The location and orientation of water molecule whose plane is parallel with the CaF_2 (111) is nearly unchanged. Nevertheless, those water molecules whose plane is vertical with CaF_2 (111) rotates slightly to form hydrogen bonds with F atoms. The unit cell is still the six-numbered planar ring, and the hydrogen bond network is the same with ice II which satisfy the ice rule.

Different from ice II, monolayer ice III is composed of planar rhombic rings and all the water molecules tilt with respect to the plane of oxygen. When intercalated into CaF_2 (111) and graphene, it distorts slightly. The four-membered unit cell almost remains unchanged, but the orientations of water molecules become disorganized and delamination appears. Unlike ice II-III, oxygen atoms of ice IV are in alternative ridges with different height in the normal direction. Under confinement, the unit cell of ice IV also changes from rhombic to four-and five-membered rings (**Figure 2C**).

Ice Ih is also intercalated into the CaF_2 (111) and graphene. Two cases of ice Ih are tried as shown in **Figures 2D,E**. In the **Figure 2D**, all the hydrogen atoms are pointing to the graphene coating, while in the **Figure 2E**, all the hydrogen atoms are pointing to the CaF_2(111). These two ice configurations are called "Ih-up" and "Ih-down," respectively. In the two cases, the ice structure nearly remains unchanged. The hydrogen atoms tend to point to the CaF_2 (111), so in the structure of "Ih-up," some water molecules rotate to point to the CaF_2 (111).

To further determine the stability of these monolayer ice phases when they are confined between CaF_2 (111) and the graphene system, the binding energies of monolayer ice phases between the CaF_2 and the graphene system are calculated *via* **Eq. 1**. The results are shown in **Figure 2F**. Clearly, the stability sequence is: III (−0.851 eV/H_2O) > IV (−0.744 eV/H_2O) > II (−0.738 eV/H_2O) ≈ Ih-up (−0.739 eV/H_2O) ≈ Ih-down (−0.733 eV/H_2O). Intriguingly, ice III possesses largest binding energy (−0.85 eV/H_2O), demonstrating its high stability confined between CaF_2 (111) and graphene. Moreover, we have also tried several amorphous water structures in this confined system by random distributing the water molecules. As shown in **Supplementary Figure S2**, the amorphous water layers retain a monolayer character. But these two amorphous structures are less stable than ordered ice phases. The stability sequence is: III (−0.851 eV/H_2O) > IV (−0.744 eV/H_2O) > II (−0.738 eV/H_2O) ≈ Ih-up (−0.739 eV/H_2O) ≈ Ih-down (−0.733 eV/H_2O) > Amor-1 (**Supplementary Figure S2A**) (−0.65 eV/H_2O) > Amor-2 (**Supplementary Figure S2B**) (−0.55 eV/H_2O).

To understand the stability and structural properties through electronic properties, the band structures of the CaF_2/graphene system and five ice phases confined between CaF_2 (111) and graphene are presented in **Figures 3A–F**, respectively. Due to the different size of the graphene's supercell, the location of Dirac cone is distinct. The contribution from graphene and CaF_2 (111) is plotted in **Figure 3A**. Before ice intercalation, the gap of CaF_2 (111) bands is about 6.35 eV; while in the ice confined systems, the gap changes slightly, in the range of (5.5, 6.18) eV. Additionally, in CaF_2 (111)/II/graphene and CaF_2 (111)/Ih-down/graphene, the CaF_2 (111) bands both move downward probably because most H atoms point to the CaF_2 (111) surface. The contribution to each band from ice phases

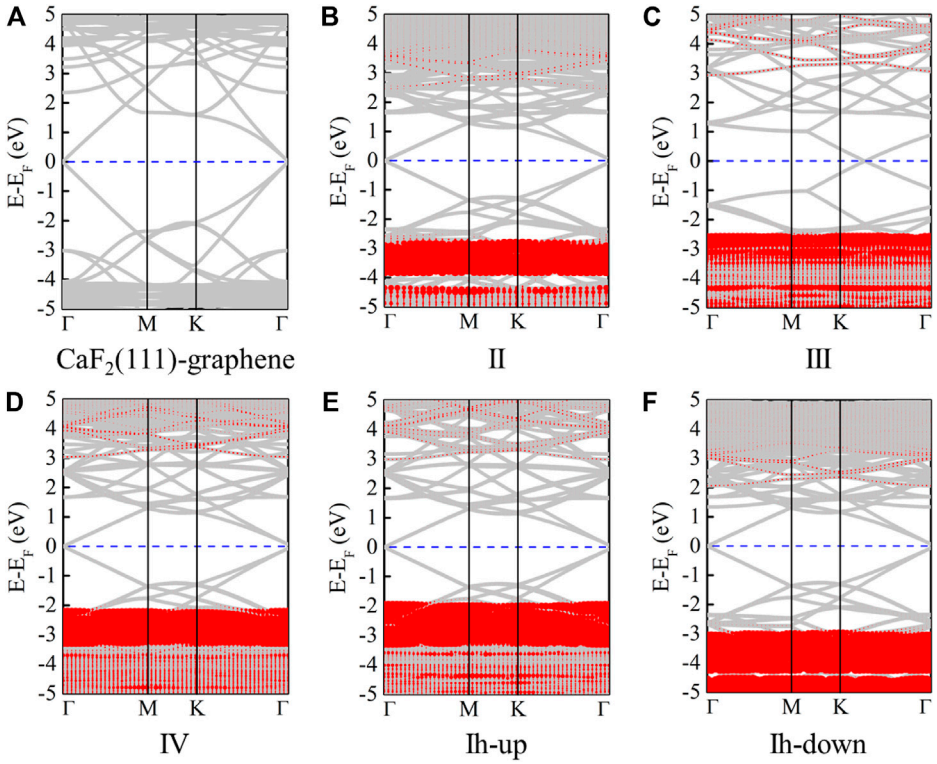

FIGURE 3 | Band structures of CaF_2 (111)/graphene **(A)**, CaF_2 (111)/II/graphene **(B)**, CaF_2 (111)/III/graphene **(C)**, CaF_2 (111)/IV/graphene **(D)**, CaF_2 (111)/Ih-up/graphene **(E)**, and CaF_2 (111)/Ih-down/graphene **(F)**, respectively. Here, the red parts represent the contribution from monolayer ice. The Fermi levels are set to zero and indicated by the blue line.

are all depicted in **Figures 3B–F**. For these five ice phases, band dispersion is very flat along the high symmetry directions in the Brillouin zone. Besides, the ice bands are all located at the deep energy level at least 2–3 eV lower than the Fermi level. Similarly, due to the orientation of H atoms, the locations of bands originated from ice II and ice Ih-down are the deepest among these five ice phases [(−3.79, −2.93) (−5.36, −3.02) eV].

Phase Diagram

Binding energy results demonstrate the highly kinetic stability of ice III; nevertheless, under real environment, the water pressure and temperature must be considered. Based on first-principles thermodynamic calculations [47–50], the free Gibbs energy change ΔG of the CaF_2 (111)/ice III/graphene confined system is defined as:

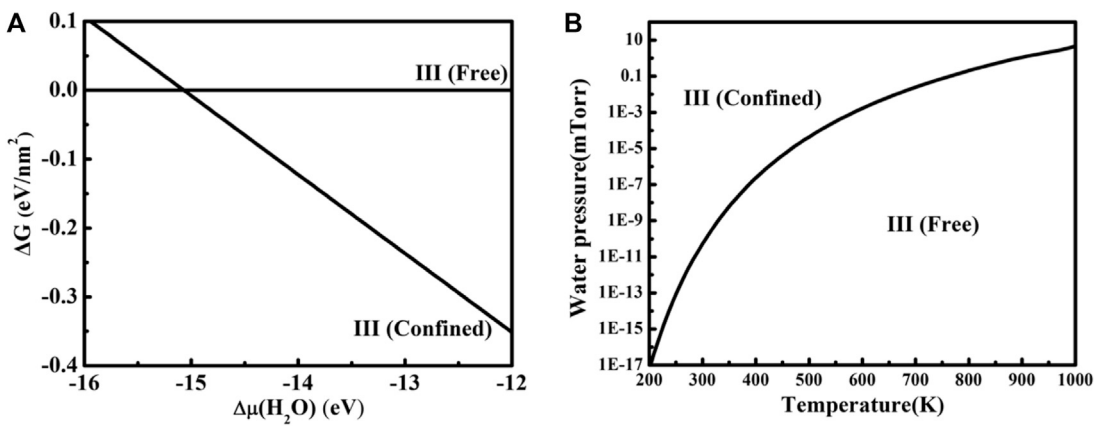

FIGURE 4 | (A) Gibbs free energy change ΔG for freestanding ice III and the CaF_2 (111)/ice III/graphene system *versus* the chemical potential change of the gas water molecule. **(B)** The phase diagram for free standing ice III and the CaF_2 (111)/ice III/graphene system under different P and T.

$$\Delta G = \left[E(\text{Total}) - E(CaF_2) - E(\text{Graphene}) - N(H_2O) * \Delta\mu(H_2O)\right]/A, \quad (3)$$

where $E(\text{Total})$, $E(CaF_2)$, $E(\text{Graphene})$, and $E(H_2O)$ is total energy of the CaF_2/H_2O/graphene system, clean CaF_2 (111), graphene sheet, and isolated water molecule, respectively. A is the surface area and $N(H_2O)$ is the number of the water molecules included in the ice phases. $\Delta\mu(H_2O)$ is the chemical potentials of water in gas phase, which can be associated with the DFT results and experimental thermodynamic data, as follows:

$$\Delta\mu(H_2O) = E(H_2O) + \mu_g(P^0, T) - K_b T ln\left[P_g(H_2O)/P^0\right], \quad (4)$$

where P^0 = 1 bar and the $\mu_g(P_0, T)$ represents the standard chemical potential of gas water, which can be obtained from standard thermodynamic tables [51].

The free Gibbs energy change ΔG of freestanding ice III [III(free)] and the CaF_2(111)/ice III/graphene [III(confined)] system is depicted in **Figure 4A** using **Eq. 3**. When $\Delta\mu(H_2O)$ is lower than −15.07 eV, ice III is not likely to be confined between CaF_2(111) and graphene. On the contrary, the confined system will be more favorable. According to **Eq. 4** and the phase transition value of $\Delta\mu(H_2O)$ obtained from **Figure 4B**, a two-dimensional (*T, P*) phase diagram is further plotted. Ice III tends to be confined between CaF_2 (111) and graphene under a wide T and P span. For example, at room temperature, confined ice III is more thermodynamically favorable when the water pressure is larger than 10^{-10} mTorr. However, the condition for freestanding ice III is harsh, often under ultra-high vacuum. Noted that all our configurations were obtained without compression, applying the compression to reduce the layer distance between graphene and CaF_2 could further tune the structure and stability of water layer, which deserves comprehensive study in the future.

CONCLUSION

In conclusion, we have theoretically studied the structure and stability of monolayer ice phases confined between CaF_2 (111) and graphene. The stratification test and CI-NEB calculations demonstrate the possibility of monolayer ice formation in the CaF_2 (111) and graphene system. Therefore, five systems including monolayer ice II, III, IV, I_h-up, and I_h-down confined between CaF_2(111) and graphene are considered. After optimization, all the ice phases undergo very small deformation, indicating that the 2D monolayer ice can be stable in the CaF_2–graphene–confined system. The electronic properties of these five systems are calculated. Nearly all the bands originated from confined ice are flat and locate about 2–3 eV below the Fermi level. By comparing the binding energy of five systems, the stability sequence is identified as: III > IV > II ≈ Ih-up ≈ Ih-down. Beyond, based on first-principles thermodynamic calculations, a two-dimensional (*T*, *P*) phase diagram for III(free) and III(confined) is further plotted. Ice III tends to be confined between CaF_2 (111) and graphene under a wide T and P range.

DATA AVAILABILITY STATEMENT

The raw data supporting the conclusions of this article will be made available by the authors, without undue reservation.

AUTHOR CONTRIBUTIONS

JG and S-QL proposed this study. S-QL and SQ performed simulation. JG, HL, and MC conducted the studies and discussed the result. All authors wrote and revised this paper.

FUNDING

This work was financially supported by the National Natural Science Foundation of China (Nos. 12074053, 91961204, and 11664028) and by Xin Liao Ying Cai Project of the Liaoning Province, China (XLYC1907163). JG thanks the Start-Up grant of DUT (DUT20RC(5)026).

ACKNOWLEDGMENTS

We also acknowledge the computers supporting from the Shanghai Supercomputer Center, the DUT supercomputing Center, and Tianhe supercomputer of Tianjin Center.

SUPPLEMENTARY MATERIAL

The Supplementary Material for this article can be found online at: https://www.frontiersin.org/articles/10.3389/fphy.2021.740627/full#supplementary-material

REFERENCES

1. Soper AK. THERMODYNAMICS: Enhanced: Water and Ice. *Science* (2002) 297:1288–9. doi:10.1126/science.297.5585.1288
2. Zangi R, and Mark AE. Monolayer Ice. *Phys Rev Lett* (2003) 91:025502. doi:10.1103/PhysRevLett.91.025502
3. Qiu H, and Guo W. Electromelting of Confined Monolayer Ice. *Phys Rev Lett* (2013) 110:195701. doi:10.1103/physrevlett.110.195701
4. Chen J, Schusteritsch G, Pickard CJ, Salzmann CG, and Michaelides A. Two Dimensional Ice from First Principles: Structures and Phase Transitions. *Phys Rev Lett* (2016) 116:025501. doi:10.1103/PhysRevLett.116.025501
5. Rasaiah JC, Garde S, and Hummer G. Water in Nonpolar Confinement: from Nanotubes to Proteins and beyond. *Annu Rev Phys Chem* (2008) 59:713–40. doi:10.1146/annurev.physchem.59.032607.093815
6. Asay DB, and Kim SH. Evolution of the Adsorbed Water Layer Structure on Silicon Oxide at Room Temperature. *J Phys Chem B* (2005) 109(35):16760–3. doi:10.1021/jp053042o

7. Zhang Y, Nappini S, Sankar R, Bondino F, Gao J, and Politano A. Assessing the Stability of Cd3As2 Dirac Semimetal in Humid Environments: the Influence of Defects, Steps and Surface Oxidation. *J Mater Chem C* (2021) 9:1235–44. doi:10.1039/d0tc04883f
8. Centi G. Smart Catalytic Materials for Energy Transition. *SmartMat* (2020) 1: e1005. doi:10.1002/smm2.1005
9. Giovambattista N, Rossky PJ, and Debenedetti PG. Effect of Pressure on the Phase Behavior and Structure of Water Confined between Nanoscale Hydrophobic and Hydrophilic Plates. *Phys Rev E Stat Nonlin Soft Matter Phys* (2006) 73:041604. doi:10.1103/PhysRevE.73.041604
10. Jang C, Adam S, Chen J-H, Williams ED, Das Sarma S, and Fuhrer MS. Tuning the Effective fine Structure Constant in Graphene: Opposing Effects of Dielectric Screening on Short- and Long-Range Potential Scattering. *Phys Rev Lett* (2008) 101:146805. doi:10.1103/physrevlett.101.146805
11. Shim J, Lui CH, Ko TY, Yu Y-J, Kim P, Heinz TF, et al. Water-gated Charge Doping of Graphene Induced by Mica Substrates. *Nano Lett* (2012) 12:648–54. doi:10.1021/nl2034317
12. Li S-Q, Chang Y, Zhang Z, Liu H, Chen M, Han Y, et al. Evolution of Water Layer Adsorption on the GaN(0001) Surface and its Influence on Electronic Properties. *J Phys Chem C* (2021) 125:667–74. doi:10.1021/acs.jpcc.0c10256
13. So Much More to Know. *Science*. (2005) 309: 78–102. doi:10.1126/science.309.5731.78b
14. Xu Y, Xuan X, Zhang Z, and Guo W. A Helical Monolayer Ice. *J Phys Chem Lett* (2020) 11:3860–5. doi:10.1021/acs.jpclett.0c01129
15. Ma R, Cao D, Zhu C, Tian Y, Peng J, Guo J, et al. Atomic Imaging of the Edge Structure and Growth of a Two-Dimensional Hexagonal Ice. *Nature* (2020) 577:60–3. doi:10.1038/s41586-019-1853-4
16. Chen J, Guo J, Meng X, Peng J, Sheng J, Xu L, et al. An Unconventional Bilayer Ice Structure on a NaCl(001) Film. *Nat Commun* (2014) 5:4056. doi:10.1038/ncomms5056
17. Nie S, Feibelman PJ, Bartelt NC, and Thürmer K. Pentagons and Heptagons in the First Water Layer on Pt(111). *Phys Rev Lett* (2010) 105:026102. doi:10.1103/PhysRevLett.105.026102
18. Yang J, Meng S, Xu LF, and Wang EG. Ice Tessellation on a Hydroxylated Silica Surface. *Phys Rev Lett* (2004) 92:146102. doi:10.1103/physrevlett.92.146102
19. Algara-Siller G, Lehtinen O, Wang FC, Nair RR, Kaiser U, Wu HA, et al. Square Ice in Graphene Nanocapillaries. *Nature* (2015) 519:443–5. doi:10.1038/nature14295
20. Xu K, Cao P, and Heath JR. Graphene Visualizes the First Water Adlayers on Mica at Ambient Conditions. *Science* (2010) 329:1188–91. doi:10.1126/science.1192907
21. Matheswaran P, Gokul B, Abhirami KM, and Sathyamoorthy R. Thickness Dependent Structural and Optical Properties of In/Te Bilayer Thin Films. *Mater Sci Semiconductor Process* (2012) 15:486–91. doi:10.1016/j.mssp.2012.03.006
22. Ochedowski O, Bussmann BK, and Schleberger M. Graphene on Mica - Intercalated Water Trapped for Life. *Sci Rep* (2014) 4:6003. doi:10.1038/srep06003
23. Rezania B, Dorn M, Severin N, and Rabe JP. Influence of Graphene Exfoliation on the Properties of Water-Containing Adlayers Visualized by Graphenes and Scanning Force Microscopy. *J Colloid Interf Sci* (2013) 407:500–4. doi:10.1016/j.jcis.2013.06.034
24. Severin N, Lange P, Sokolov IM, and Rabe JP. Reversible Dewetting of a Molecularly Thin Fluid Water Film in a Soft Graphene-Mica Slit Pore. *Nano Lett* (2012) 12:774–9. doi:10.1021/nl2037358
25. Lee D, Ahn G, and Ryu S. Two-Dimensional Water Diffusion at a Graphene-Silica Interface. *J Am Chem Soc* (2014) 136:6634–42. doi:10.1021/ja4121988
26. Lee MJ, Choi JS, Kim J-S, Byun I-S, Lee DH, Ryu S, et al. Characteristics and Effects of Diffused Water between Graphene and a SiO2 Substrate. *Nano Res* (2012) 5:710–7. doi:10.1007/s12274-012-0255-9
27. Verdaguer A, Segura JJ, López-Mir L, Sauthier G, and Fraxedas J. Communication: Growing Room Temperature Ice with Graphene. *J Chem Phys* (2013) 138:121101. doi:10.1063/1.4798941
28. Kazakova O, Panchal V, and Burnett T. Epitaxial Graphene and Graphene-Based Devices Studied by Electrical Scanning Probe Microscopy. *Crystals* (2013) 3:191–233. doi:10.3390/cryst3010191
29. Komurasaki H, Tsukamoto T, Yamazaki K, and Ogino T. Layered Structures of Interfacial Water and Their Effects on Raman Spectra in Graphene-On-Sapphire Systems. *J Phys Chem C* (2012) 116:10084–9. doi:10.1021/jp301402u
30. Xu Z, Ao Z, Chu D, Younis A, Li CM, and Li S. Reversible Hydrophobic to Hydrophilic Transition in Graphene *via* Water Splitting Induced by UV Irradiation. *Sci Rep* (2014) 4:6450. doi:10.1038/srep06450
31. Feng X, Maier S, and Salmeron M. Water Splits Epitaxial Graphene and Intercalates. *J Am Chem Soc* (2012) 134:5662–8. doi:10.1021/ja3003809
32. Ochedowski O, Begall G, Scheuschner N, El Kharrazi M, Maultzsch J, and Schleberger M. Graphene on Si(111)7×7. *Nanotechnology* (2012) 23:405708. doi:10.1088/0957-4484/23/40/405708
33. Temmen M, Ochedowski O, Schleberger M, Reichling M, and Bollmann TRJ. Hydration Layers Trapped between Graphene and a Hydrophilic Substrate. *New J Phys* (2014) 16:053039. doi:10.1088/1367-2630/16/5/053039
34. Bollmann TRJ, Antipina LY, Temmen M, Reichling M, and Sorokin PB. Hole-doping of Mechanically Exfoliated Graphene by Confined Hydration Layers. *Nano Res* (2015) 8:3020–6. doi:10.1007/s12274-015-0807-x
35. Xu J, Cui X, Liu N, Chen Y, and Wang HW. Structural Engineering of Graphene for High-resolution Cryo-electron Microscopy. *SmartMat* (2021) 2: 202–12. doi:10.1002/smm2.1045
36. Kresse G, and Furthmüller J. Efficient Iterative Schemes Forab Initiottotal-Energy Calculations Using a Plane-Wave Basis Set. *Phys Rev B* (1996) 54: 11169–86. doi:10.1103/physrevb.54.11169
37. Perdew JP, Burke K, and Ernzerhof M. Generalized Gradient Approximation Made Simple. *Phys Rev Lett* (1996) 77:3865–8. doi:10.1103/PhysRevLett.77.3865
38. Grimme S, Antony J, Ehrlich S, and Krieg H. A Consistent and Accurate Ab Initio Parametrization of Density Functional Dispersion Correction (DFT-D) for the 94 Elements H-Pu. *J Chem Phys* (2010) 132:154104. doi:10.1063/1.3382344
39. Kresse G, and Joubert D. From Ultrasoft Pseudopotentials to the Projector Augmented-Wave Method. *Phys Rev B* (1999) 59:1758–75. doi:10.1103/physrevb.59.1758
40. Monkhorst HJ, and Pack JD. Special Points for Brillouin-Zone Integrations. *Phys Rev B* (1976) 13:5188–92. doi:10.1103/physrevb.13.5188
41. Neugebauer J, and Scheffler M. Adsorbate-substrate and Adsorbate-Adsorbate Interactions of Na and K Adlayers on Al(111). *Phys Rev B* (1992) 46:16067–80. doi:10.1103/physrevb.46.16067
42. Krukowski S, Kempisty P, and Strąk P. Electrostatic Condition for the Termination of the Opposite Face of the Slab in Density Functional Theory Simulations of Semiconductor Surfaces. *J Appl Phys* (2009) 105: 113701. doi:10.1063/1.3130156
43. Zhao W-H, Wang L, Bai J, Yuan L-F, Yang J, and Zeng XC. Highly Confined Water: Two-Dimensional Ice, Amorphous Ice, and Clathrate Hydrates. *Acc Chem Res* (2014) 47:2505–13. doi:10.1021/ar5001549
44. Henkelman G, Uberuaga BP, and Jónsson H. A Climbing Image Nudged Elastic Band Method for Finding Saddle Points and Minimum Energy Paths. *J Chem Phys* (2000) 113:9901–4. doi:10.1063/1.1329672
45. Kang K, Morgan D, and Ceder G. First Principles Study of Li Diffusion in I-Li_2NiO_2 Structure. *Phys Rev B* (2009) 79:014305. doi:10.1103/physrevb.79.014305
46. Morgan D, Van der Ven A, and Ceder G. Li Conductivity in Li[sub x]MPO[sub 4] (M = Mn, Fe, Co, Ni) Olivine Materials. *Electrochem Solid-state Lett* (2004) 7:A30. doi:10.1149/1.1633511
47. Kowalski PM, Meyer B, and Marx D. Composition, Structure, and Stability of the rutileTiO2(110)surface: Oxygen Depletion, Hydroxylation, Hydrogen Migration, and Water Adsorption. *Phys Rev B* (2009) 79:115410. doi:10.1103/physrevb.79.115410
48. Li W, Zhao J, Zhu Q, and Wang D. Insight into the Initial Oxidation of 4H-SiC from First-Principles Thermodynamics. *Phy Rev B* (2013) 87:085320. doi:10.1103/physrevb.87.085320
49. Reuter K, and Scheffler M. First-principles Atomistic Thermodynamics for Oxidation Catalysis: Surface Phase Diagrams and Catalytically Interesting Regions. *Phys Rev Lett* (2003) 90:046103. doi:10.1103/PhysRevLett.90.046103
50. Zhang W, Wu P, Li Z, and Yang J. First-principles Thermodynamics of Graphene Growth on Cu Surfaces. *J Phys Chem C* (2011) 115:17782–7. doi:10.1021/jp2006827

51. Chase JMW. *NIST-JANAF Thermochemical Tables*. 4th ed. New York: American Institute of Physics (1998).

Conflict of Interest: The authors declare that the research was conducted in the absence of any commercial or financial relationships that could be construed as a potential conflict of interest.

Publisher's Note: All claims expressed in this article are solely those of the authors and do not necessarily represent those of their affiliated organizations, or those of the publisher, the editors, and the reviewers. Any product that may be evaluated in this article, or claim that may be made by its manufacturer, is not guaranteed or endorsed by the publisher.